PHYSICAL REVIEW D VOLUME 25, NUMBER 3 1 FEBRUARY 1982

High-transverse-momentum leptons from B mesons: Their characteristics and uses

M. J. Puhala, Z. J. Rek,* Bing-lin Young, and Xue-Tian Zhu†
Department of Physics and Ames Laboratory, Iowa State University, Ames, Iowa 50011
(Received 6 July 1981; revised manuscript received 8 September 1981)

A method for identifying bottom-quark production in e^+e^- annihilation reactions at energies above threshold (but below the top-quark threshold) is proposed. The main ingredient of this method is the high-$k_\perp$ lepton resulting from bottom-quark decays, where $k_\perp$ is the transverse momentum with respect to the jet axis. The kinematic nature of this method makes it insensitive to many uncertainties, such as jet-axis misidentification, primordial transverse momentum of the heavy mesons, gluonic corrections, etc., as verified by means of a detailed Monte Carlo calculation. The characteristics of the spectra enable one to determine the quark jet (vs the antiquark jet) direction, and the b-quark fragmentation function. We recommend and justify the use of thrust in our analysis. We discuss several applications, especially the discrimination of quark fragmentation functions.

I. INTRODUCTION

With the observation of the Υ''' at CESR,[1] the field of meson spectroscopy has reached yet another new and exciting stage. The broad width of the Υ''' (12.6 MeV) suggests that this new resonance is above the threshold for producing $B\bar{B}$ pairs, where B is a pseudoscalar meson composed of a b quark, and a $\bar{u}$ or $\bar{d}$ antiquark. The existence of B mesons has been inferred[2] from a study of the prompt-lepton energy spectrum. At e^+e^- center-of-mass energies $\sqrt{s}$ away from $b\bar{b}$ quark resonances it is much more difficult to observe bottom particles. For values of $\sqrt{s}$ well below the Z^0 mass, the ratio of bottom to charm production is approximately 1:4; thus the electrons from charmed-meson production tend to mask those from B mesons. In a previous paper[3] we described briefly a method by which jets containing B mesons can be identified, even at PEP and PETRA energies, by selecting events containing electrons or muons with high transverse momentum relative to the jet axis. We show that this method, originally suggested by others,[4] is expected to work extremely well for the case of B mesons, due to the fact that for extremely relativistic leptons, the transverse-momentum smearing, $\Delta k_\perp/k_\perp$, goes like $\langle q_\perp\rangle/m_H$, where m_H is the mass of the "parent" heavy meson and $\langle q_\perp\rangle$ is the average transverse momentum of the heavy mesons. As we will demonstrate, the most serious background, namely the semileptonic decays of the D mesons, can be eliminated. Having identified a clean sample of B-meson events, we illustrate how one can study effects such as the momentum distribution of the B's as well as γ-Z^0 interference in the PEP/PETRA energy regime. The main results of our paper will be insensitive to the assumed longitudinal- and transverse-momentum distributions of the B's and D's, due to simple kinematics.

The outline of this paper is as follows. In Sec. II, we discuss the physical picture that we employ to calculate the prompt lepton production in e^+e^- annihilation. In Sec. III, we investigate the transverse-momentum distribution of electrons with respect to the jet axis. We investigate sensitivity of the transverse-momentum spectrum to assumptions about the primordial $q_\perp$ of the hadrons, the decay modes of the B's and D's, the effects of hard-gluon emission, and experimental uncertainty in determing the jet axis. In Sec. IV, we give some applications of our methods. In Sec. V, we summarize our results.

II. MODEL FOR THE PRODUCTION OF PROMPT LEPTONS

Let us briefly describe the model used to generate prompt-lepton events in e^+e^- annihilation. The model is a variation[5] of the standard scheme proposed in the literature.[6,7] The electron and pos-

itron annihilate via either a single photon or Z^0 into a heavy-quark pair, as in the standard model. The heavy quark (c,b) then fragments into exactly one heavy meson (termed D, B, respectively) containing the parent quark, plus a number of "ordinary" hadrons. The heavy meson is created with some primordial transverse momentum with respect to the jet axis. Prompt leptons are then produced in the semileptonic decays of the heavy mesons, as well as in the decays of the D's produced by B-meson decay.

By way of definition, the production rate for flavor i is given by

$$\gamma_i = \frac{\sigma_i}{\sum_j \sigma_j} = \frac{\sigma_i}{\sigma_H} , \tag{2.1}$$

where σ_i is the cross section for producing favor i and σ_H is the hadronic cross section. Expressions for the γ_i are given in Ref. 8. The fragmentation functions for the heavy quarks to hadronize into heavy mesons are given by

$$D_i(Z,q_\perp{}^2) = D_i(Z)\frac{e^{-q_\perp{}^2/2t_H{}^2}}{2t_H{}^2} , \tag{2.2}$$

where Z is the longitudinal-momentum fraction, and $q_\perp$ the primordial transverse momentum, of the heavy meson with respect to the jet axis. We recommend the use of thrust[9] to define such an axis, for reasons that we describe in Sec. III.

The differential decay rates $(1/\Gamma_i)/d\Gamma_i/dE$ for the semileptonic decays of the heavy mesons containing heavy quark i are calculated in the quark-spectator model. We ignore gluonic corrections,[10] and incorporate Kobayashi-Maskawa[11] mixing via the set of mixing angles determined in Ref. 12, restricting ourselves to the $\cos\delta = +1$ solution throughout, although our results are insensitive to this choice. We choose the quark masses to correspond to physical particle masses, so that $m_b = 5.2$ GeV, $m_c = 1.87$ GeV, $m_s = 0.5$ GeV, $m_u = m_d = 0.14$ GeV. We assume effective branching ratios of 12% for $B \to e^- X^2$ and $\bar{D} \to e^- X$.[13]

It is straightforward to calculate the spectra for the "direct" process given in (a) and (c) of Table I. In order to calculate the prompt-electron spectrum for the "cascade" process in (b) of Table I, one must know $(1/\Gamma_{\rm NL})d\Gamma_{\rm NL}/dE_D$, the differential decay rate for a $\bar{B}$ meson to decay nonleptonically into a $\bar{D}$ meson with energy between E_D and $E_D + dE_D$ in the $\bar{B}$ rest frame. We have derived an expression by assuming that the nonleptonic decay proceeds entirely via $\bar{B} \to \bar{D} + n\pi$. If we neglect the pion mass and the dependence of the matrix element on the external momenta, we can compute the energy spectrum of the $\bar{D}$ in the rest frame of the $\bar{B}$ analytically.[5] We find that

$$\frac{1}{\Gamma_{\rm NL}}\frac{d\Gamma_{\rm NL}}{dx_D} = P(1)\delta(x_D - 1) + \sum_{n=2}^{\infty} P(n)\frac{(x_D{}^2 - x_L{}^2)^{1/2}(1-x_D)^{n-2}}{I_n(x_L)} , \tag{2.3}$$

where $P(n)$ is the pion multiplicity, and

TABLE I. Various decay modes of charm and bottom mesons leading to electrons in the final state.

(a)	$B \to D e^- \bar{\nu}$
(b)	$\bar{B} \to \bar{D} X \to K e^- \bar{\nu}$
(c)	$\bar{D} \to K e^- \bar{\nu}$
(d)	$B^* \to B X \to D e^- \bar{\nu}$
(e)	$B^* \to B X \to D^* e^- \bar{\nu}$
(f)	$\bar{B}^* \to \bar{B} X \to \bar{D} X' \to K e^- \bar{\nu}$
(g)	$\bar{B}^* \to \bar{B} X \to \bar{D}^* X' \to \bar{D} X'' \to K e^- \bar{\nu}$
(h)	$\bar{B}^* \to \bar{B} X \to \bar{D} X' \to K^* e^- \bar{\nu}$
(i)	$\bar{B}^* \to \bar{B} X \to \bar{D}^* X' \to \bar{D} X'' \to K^* e^- \bar{\nu}$
(j)	$\bar{D}^* \to \bar{D} X \to K e^- \bar{\nu}$
(k)	$\bar{D}^* \to \bar{D} X \to K^* e^- \bar{\nu}$
(l)	$B \to D^* e^- \bar{\nu}$
(m)	$\bar{B} \to \bar{D}^* X \to \bar{D} X' \to K e^- \bar{\nu}$
(n)	$\bar{B} \to \bar{D} X \to K^* e^- \bar{\nu}$
(o)	$\bar{B} \to \bar{D}^* X \to \bar{D} X' \to K^* e^- \bar{\nu}$
(p)	$\bar{D} \to K^* e^- \bar{\nu}$

$$x_D=\frac{2m_bE_D}{m_b^2+m_c^2}\ , \tag{2.4}$$

$$x_L=\frac{2m_bm_c}{m_b^2+m_c^2}\ , \tag{2.5}$$

$$I_n(x_L)\equiv\int_{x_L}^1 dy(y^2-x_L^2)^{1/2}(1-y)^{n-2}\ . \tag{2.6}$$

We assume that $P(n)$ is Poisson-type with an average multiplicity $\langle n\rangle=4$ as deduced from low-energy e^+e^- data.[23]

III. CHARACTERISTICS OF THE HIGH-$k_\perp$ SPECTRUM

As we have mentioned, our main results will be insensitive to the choice of longitudinal-mometum spectrum $D_i(z)$. Perturbative QCD gives little clue as to the appropriate choice of the fragmentation functions $D_i(z)$. Fortunately, the study of high-transverse-momentum electrons will yield information about the form of the fragmentation functions, as we will shortly see. To simplify our discussion, we shall assume that $D_i(z)$ is independent of the heavy-flavor index i, unless otherwise stated. It is generally believed that the fragmentation functions may lie between two types. The first assumes that the fragmentation functions for heavy quarks into heavy hadrons are similar to those for "light" quarks (u,d,s) into "light" hadrons (K's and π's). This is the fragmentation model of Field and Feynman[14] (FF)

$$D(z)=1-a+3a(1-x)^2\ . \tag{3.1}$$

Recent fits[15] of PETRA data yield $a=0.57$. This corresponds to a soft fragmentation, peaking at $z=0$. In contrast to this picture, Bjorken and Suzuki[16] (BS) have argued that the fragmentation function for a heavy quark to fragment into a heavy meson should be hard peaked near $z=1$. It has been suggested that[16]

$$D(z)=2z\ . \tag{3.2}$$

Although our main results are insensitive to the choice of $D(z)$, a study of the high-$k_\perp$ electrons can distinguish (3.1) from (3.2).

As has been pointed out previously,[3,4] prompt electrons from B mesons tend to be hidden by the electrons from $\bar{D}$ decay. From Eq. (2.1), we calculate that for $\sqrt{s}=31$ GeV,

$$\begin{aligned}\sigma_H&=0.33\text{ nb}\ ,\\ \gamma_c&=0.36\ ,\\ \gamma_b&=0.09\ .\end{aligned} \tag{3.3}$$

In Fig. 1, we show a calculation of $d\sigma_e/dE^c$ at this energy, where E^c is the electron energy in the e^+e^- center-of-mass frame. For illustrative purposes, we have chosen a fragmentation function of the type (3.1) for the D mesons, and of the form (3.2) for the B mesons. This choice, which corresponds to the maximum possible separation of the B and $\bar{D}$ electron energy spectra, yields an electron energy spectrum that is dominated by the electrons from the semileptonic decays of the $\bar{D}$'s throughout the entire range of E^c. One does not expect any distinctive way to separate B mesons from the $\bar{D}$ mesons in $d\sigma_e/dE^c$ off resonance until $\gamma_c\approx\gamma_b$, which occurs near $\sqrt{s}=80$ GeV. If the $\bar{D}$-meson fragmentation function is harder than

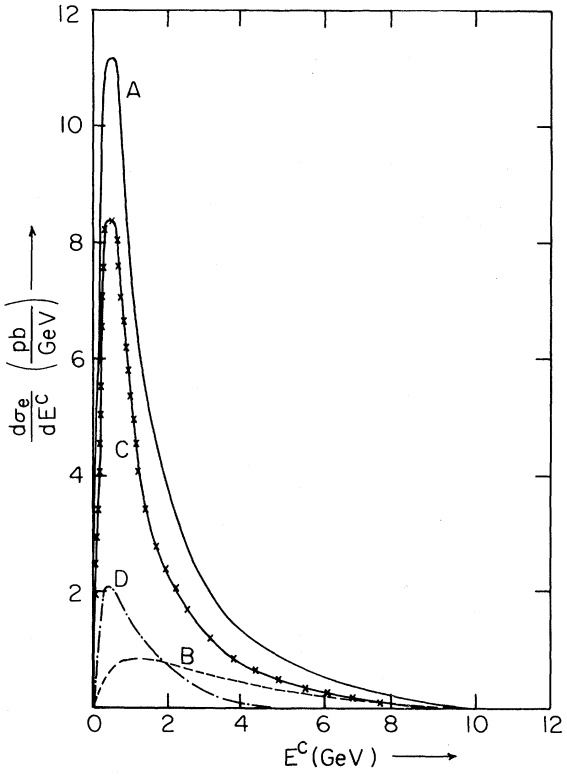

FIG. 1. Prompt-electron energy spectrum $d\sigma_e/dE^c$ for $\sqrt{s}=31$ GeV. FF fragmentation function for charm; BS fragmentation function for bottom. Curve A, total; curve B, bottom contributon; curve C, charm; curve D, cascade.

(3.1), or if the B-meson fragmentation function is softer than (3.2), then the B will be even harder to detect using the $d\sigma_e/dE^c$ spectrum.

We propose that clear evidence of B-meson production should be obtained by examining $d\sigma_e/dk_\perp$, where $k_\perp$ is the component of the observed elec tron's momentum perpendicular to the quark jet axis. In Fig. 2, we show $d\sigma_e/dk_\perp$ for $t_H=0.45$ GeV/c. Curve A shows the total electron spectrum, while curves B, C, and D show the respective contributions of bottom, charm, and cascade. The direct decays of B mesons dominate the region of high $k_\perp$, while the $\bar{D}$ and cascade contributions vanish quite rapidly for $k_\perp > 1$ GeV. In order to display the strength of the bottom signal, as well as obtain a simple measure of the charm contamination, we introduce the following quantities:

$$\sigma_{q\to e}(k_\perp)\equiv\int_{k_\perp}^{\infty}\frac{d\sigma_{q\to e}}{dk_\perp}dk_\perp,\quad q=b,\bar{c}\,, \tag{3.4}$$

$$F_q(k_\perp)\equiv\frac{\sigma_{q\to e}(k_\perp)}{\sigma_{q\to e}(k_\perp=0)},\quad q=b,\bar{c}\,, \tag{3.5}$$

$$I(k_\perp)\equiv\frac{\sigma_{\bar{c}\to e}(k_\perp)}{\sigma_{b\to e}(k_\perp)+\sigma_{\bar{c}\to e}(k_\perp)}\,. \tag{3.6}$$

We see that $F_b(k_\perp)$ $[F_{\bar{c}}(k_\perp)]$ gives the fraction of direct electrons from bottom (charm) to the total number of direct bottom (charm) electrons. The function $I(k_\perp)$ gives the fraction of charm contamination in the bottom electron sample. We shall use the above to investigate the model dependence of our results.

Let us first examine the primordial-transverse-momentum dependence. In e^+e^- reactions, it is argued[17] that jet broadening due to hard-gluon emission effectively raises the average transverse momentum of hadrons linearly with $\sqrt{s}$, causing the growth of t_H from its low-energy value of 0.3 GeV/c to 0.45 GeV/c at $\sqrt{s}=31$ GeV. It is not clear, however, whether we should regard the $\bar{D}$'s and B's as "average" hadrons, possessing the same t_H as π's or K's. Clearly, hard-gluon bremsstrahlung from heavy quarks is suppressed by mass effects, and so we expect this mechanism should cause a smaller rise in t_H for the B's and $\bar{D}$'s than the π's and K's. Also, if one believes that soft-gluon bremsstrahlung is responsible for generating the "true" primordial transverse momentum, which is the experimentally determined t_H for light mesons, it again seems that a t_H value somewhat lower than 0.45 GeV/c is appropriate. Since we are only interested in bottom and regard the $\bar{D}$'s as a background we consider the choices $t_H=0.45$ GeV/c and $t_H=0.8$ GeV/c, the latter value corresponding to a large smearing. Figures 3–5 illustrate the effects of varying t_H. In Fig. 3 we show $F_b(k_\perp)$ for $t_H=0.45$ GeV/c (solid line) and $t_H=0.8$ GeV/c (dashed lines). It is quite evident that varying t_H has little effect on the $k_\perp$ distribution of B electrons due to the fact that the B mesons are heavy and the electrons are light. In Fig.

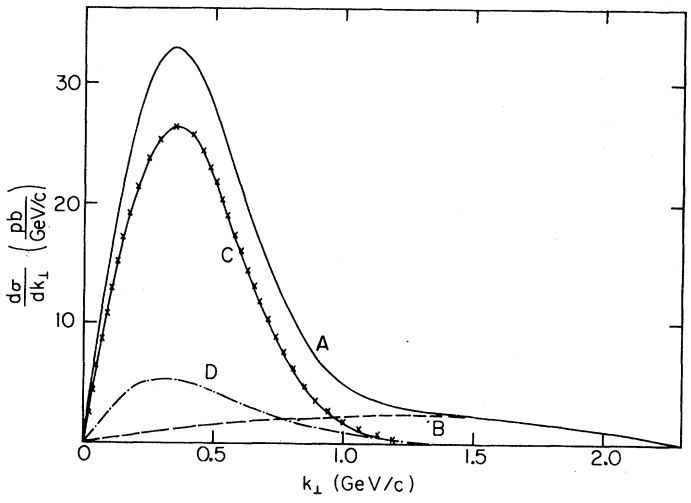

FIG. 2. Prompt-electron transverse-momentum distribution with respect to the jet axis $d\sigma_e/dk_\perp$ for $\sqrt{s}=31$ GeV. Curve A, total; curve B, bottom contribution; curve C, charm; curve D, cascade.

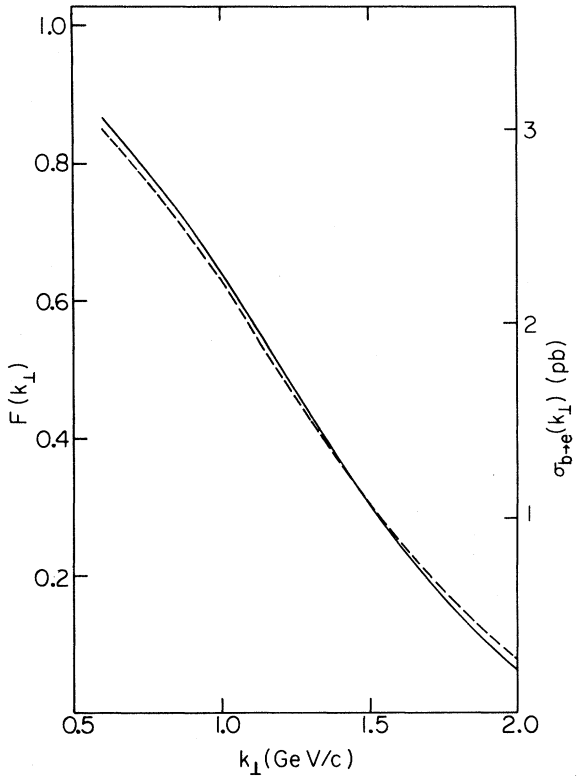

FIG. 3. Left axis: fraction of total direct electrons from bottom with transverse momentum greater than $k_\perp$. Right axis: integrated electron cross section for transverse momentum greater than $k_\perp$ at $\sqrt{s}=31$ GeV. Solid line: $t_H=0.45$ GeV/c. Dashed line: $t_H=0.8$ GeV/c.

4, we show $I(k_\perp)$. Curve A, which corresponds to $t_H=0.45$ GeV/c, yields a 2% contamination from charm for a suggested cut of $k_\perp \geq 1.2$ GeV/c; curve B, corresponding to $t_H=0.8$ GeV/c, yields a 20% contamination. The spectrum from charm is more sensitive to the choice of t_H due to the light mass of the $\bar{D}$. In order to compare the bottom and charm dependence on t_H, we plot $F_c(k_\perp)$ in Fig. 5.

So far, we have shown only the decay modes (a), (b), and (c) in Table I for the pseudoscalar mesons. We have ignored K^*, D^*, and possibly B^* production. For the sake of discussion, we enumerate all possible Cabibbo-favored decay schemes in Table I. Experimental fits to the electron spectrum of the D semileptonic decays show that the decay modes (c) and (p) are equally likely. However, the effect of including (p) is to merely soften the charm $k_\perp$ spectrum. At first, this would seem to suggest that we have overestimated the charm contamination in Fig. 4. On the other hand, since roughly equal amounts of $\bar{D}$ and $\bar{D}^*$ are produced at high energies,[13] we should use equal amounts of (c), (i), (k), and (p) to describe the electron spectrum from charm, which tends to make the electron spectrum from charm harder than just the (c) and (p) contribution. It is clear that the effects on the charm due to the inclusion of K^* modes in the final states would compensate for the effects of including D^* in the initial states. Similarly, if we assume $m_{B^*}-m_B=m_{D^*}-m_D\cong m_\pi$, then we expect that the spectrum resulting from the inclusion of equal contributions from (a), (d), (e), and (l) resembles just that of (a) alone. In order to estimate the maximum possible effects on the spectra, we ignore the decay modes $D^*\to D\pi$, $D^*\to D\gamma$, $B^*\to B\pi$, $B^*\to B\gamma$, and treat the D^* and B^* as having direct semileptonic decays, rather than decaying via the cascade. The behavior of the bottom electron spectrum is summarized by Fig. 6, where we plot $F_b(k_\perp)$ for (a), (d), and (l). The curve for (e) lies between that of (a) and (d). We conclude that the effects of including the B^* and D^* cancel in the bottom electron $k_\perp$ spectrum.

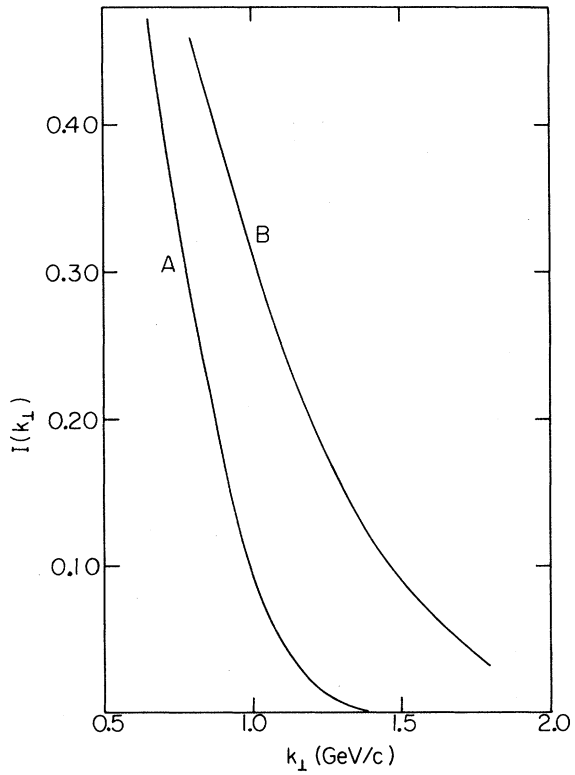

FIG. 4. Contamination function, $I(k_\perp)$. Curve A, $t_H=0.45$ GeV/c; curve B, $t_H=0.8$ GeV/c.

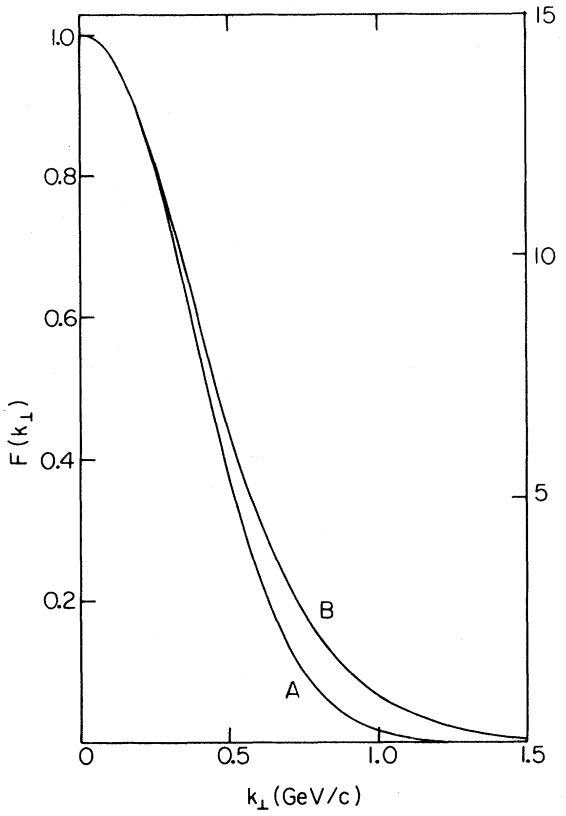

FIG. 5. Left axis: fraction of direct electrons from charm meson with transverse momentum greater than $k_\perp$. Right axis: integrated cross section for direct electrons from charm meson with transverse momentum greater than $k_\perp$.

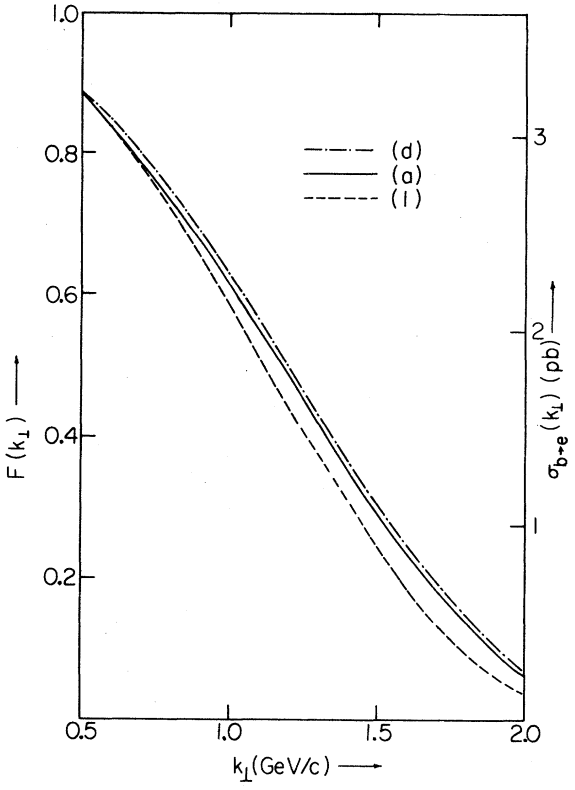

FIG. 6. Effect of various decay modes on bottom electrons (see Table I).

The effects of the various decay modes on the charm contamination of the $k_\perp$ spectrum can be summarized as follows: pure (e), (i), and (k) have less charm contamination than pure (a), (b), and (c). The effects of including the K^* more than compensates for the effects including the D^* since $m_{K^*}-m_K >> m_{D^*}-m_D$. We conclude that considering just the modes (a), (b), and (c) should yield an excellent description of $d\sigma_e/dk_\perp$ for high $k_\perp$.

The following are three important points in the determination of $d\sigma_e/dk_\perp$ under realistic conditions. First, although we have assumed that the longitudinal- and transverse-momentum dependence factorize in Eq. (2.2), this assumption is not critical due to the insensitivity of our results to the choice of t_H. Second, we have not explicitly taken into account the effect of hard-gluon bremsstrahlung off the heavy quarks. In addition to spoiling the factorization, it introduces a small, but qualitative change in the $q_\perp{}^2$ distribution of the heavy mesons. Third, we have not taken into account the smearing of the bottom and charm distributions due to experimental uncertainties in the location of the jet axis. This uncertainty is due to, among other sources, failure of the apparatus to detect neutral particles. We shall now discuss all three points.

Let us start with the second point above, namely, the effects of hard-gluon bremsstrahlung in $e^+e^-\to Q\bar{Q}G$ on the electron $k_\perp$ distribution. The thrust axis may coincide with either the Q, $\bar{Q}$, or G directions (ignoring for the time being primordial $q_\perp$, missing neutrals, etc.). If we let E_1, E_2, and E_3 be the energies of the Q, $\bar{Q}$, and G in the e^+e^- center of mass, we define the variable $Z_i \equiv 2E_i/\sqrt{s}$. The cross section for $e^+e^-\to\gamma+Q\bar{Q}G$ is given by[18]

$$\frac{d\sigma_{Q\bar{Q}G}}{dZ_1 dZ_2} = \frac{4\pi\alpha^2}{s} e_Q{}^2 \frac{2\alpha_s}{3\pi} \left[\frac{Z_1{}^2+Z_2{}^2}{(1-Z_1)(1-Z_2)} - \frac{4m_Q{}^2}{s} \left[\frac{1}{1-Z_1} + \frac{1}{1-Z_2} \right] - \frac{2m_Q{}^2}{s} \left[\frac{1}{(1-Z_1)^2} + \frac{1}{(1-Z_2)^2} \right] - \frac{4m_Q{}^4}{s^2} \left[\frac{1}{1-Z_1} + \frac{1}{1-Z_2} \right]^2 \right], \quad (3.7)$$

where m_Q is the heavy-quark mass. If we convolute (3.7) with the appropriate heavy-quark fragmentation function, we can calculate the QCD prediction for the transverse-momentum spectrum of the heavy mesons $d\sigma_Q^H/dq_\perp{}^2$. The method we use for calculating the $q_\perp{}^2$ distribution of the mesons has been described in the literature.[19]

We point out that gluon bremsstrahlung induces longitudinal-transverse momentum correlations for the heavy mesons. As we will see these correlations will reduce the smearing of the $k_\perp$ distributions due to experimental uncertainties in the location of the jet axis. The Z_1, Z_2 integration is constrained by not only the usual phase-space restrictions, but in addition we impose the cut $T < T_0$, where T is the thrust variable. This cut is necessary to avoid the divergences at $Z_i = 1$ in (3.7). Following others,[19] we take $T_0 = 0.95$ at $\sqrt{s} = 31$ GeV. We will comment later on other possible choices. As in Ref. 19, we take $t_H = 0.30$ GeV/c, and compute the transverse-momentum distribution of the heavy mesons with respect to the thrust axis. In Fig. 7, we show $d\sigma/dq_\perp{}^2$ for the $\bar{D}$ mesons, compared with TASSO data for all hadrons, which consist mainly of observed pions and kaons. We have normalized the cross sections to agree at $q_\perp{}^2 = 0$. It is evident that although gluon radiation produces a broad tail in the $q_\perp{}^2$ distribution, the tail is smaller than the $q_\perp{}^2 = 0$ value by 2 orders of magnitude. To appreciate the statistical insignificance of the gluon tail, the curve should be plotted on a linear, rather than a logarithmic scale. We note the following results:

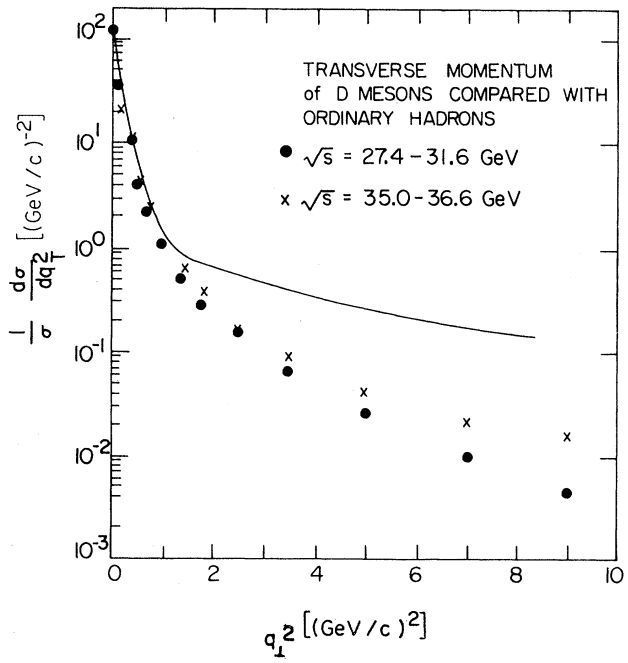

FIG. 7. Calculated curve for $\bar{D}$-meson transverse momentum. Data points taken from Ref. 20.

1. The $\bar{D}$-meson distribution is similar to the effective Gaussian parametrization in (2.2).

2. Our distributions for the $\bar{D}$'s and B's are somewhat broader than the data for the K's and π's. This is due to the fact that the heavy mesons are assumed to carry a large fraction of the longitudinal momentum of the $\bar{c}$ and b quark jets. A calculation of the $q_\perp{}^2$ distribution using $D(z) = 3(1-z)^2$, for example, produces a curve that lies somewhat below the solid curve in Fig. 7.

3. For fixed thrust cutoff T_0 the fraction of three-jet events decreases as $m_Q{}^2/s$ increases. For example, with our choice $T_0 = 0.95$ as $\sqrt{s} = 31$ GeV, we have

$$\begin{aligned} &u,d\text{: } 32\%\ , \\ &c\text{: } 30\%\ , \\ &b\text{: } 21\%\ , \end{aligned} \quad (3.8)$$

The above numbers follow from our choice of $\alpha_s = 0.18$, and our choice of the *same* T_0 for each flavor, as in Ref. 19.

The true $q_\perp{}^2$ distribution of the $\bar{D}$ mesons may deviate from the curve in Fig. 7. This could occur for several reasons. For example, we could choose a different cutoff procedure for the $Q\bar{Q}G$ amplitude, so that the total e^+e^- hadronic data is well fitted, although the distributions pertaining to indi-

vidual flavors might be altered. For example, the cut $T_0=0.95$ was obtained[20] by finding a maximum in the thrust distribution of all two-jet events, averaged over all flavors. If one were to follow such a procedure for each individual flavor, one would find that the thrust distributions are peaked at lower values of T_0 for the heavy-quark flavors. Alternative cutoff procedures, such as cutting on the minimum energy of the jet, also suggest a lower value of T_0 for the heavy quarks than for the light quarks. Until the role of nonperturbative effects is understood, it is difficult to give precise meaning to the numbers in (3.8). We shall regard them, however, as suggestive of the fact that hard-gluon bremsstrahlung for the case of heavy quarks is no more important than in the case of light quarks. In light of the possible alternative schemes for calculation that we suggested above, we will regard the curve in Fig. 7 as an upper estimate to the strength of the gluon tail.

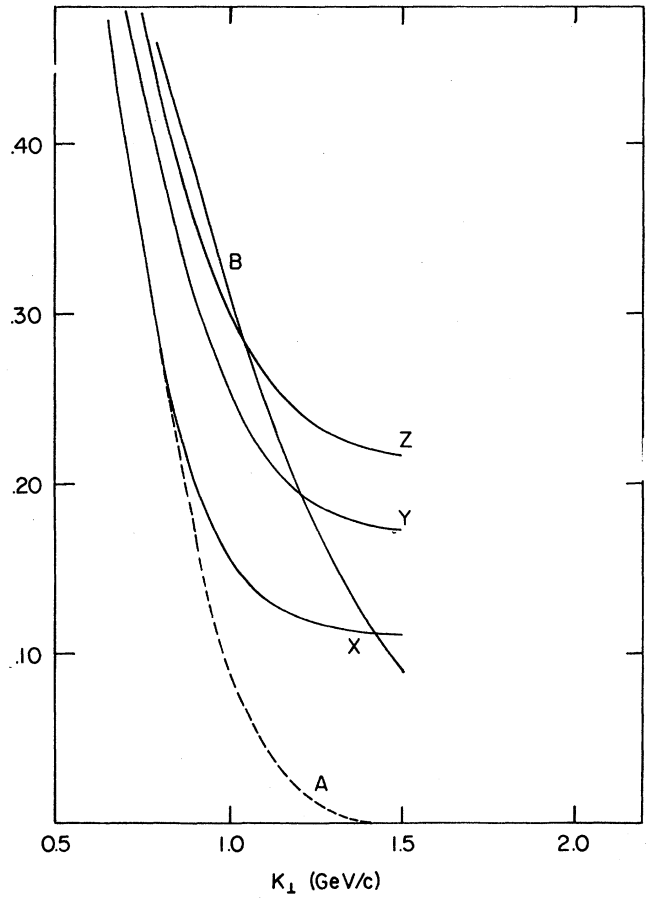

FIG. 8. Contamination function $I(k_\perp)$. Curves A and B, same as Fig. 4. Curve X includes gluon effects only. Curve Y includes gluons and jet-axis smearing for FF. Curve Z includes gluons and jet-axis smearing for $D(z)=1$.

Owing to the mass of the b quark, the function $F_b(k_\perp)$ is insensitive to the presence of the gluon tail. These kinematic effects are not as pronounced in the case of charm, and the effect of including hard-gluon emission is mainly seen through the contamination function $I(k_\perp)$. In curve X of Fig. 8, we show the resultant $I(k_\perp)$ obtained by including the meson transverse-momentum distribution resulting from (3.7). For $k_\perp=1.2$ GeV/c, we obtain $I(k_\perp)=10\%$. In light of our discussion about the hard-gluon effects, we expect, to find for $k_\perp \geq 1.2$ GeV/c, $2-11\%$ charm contamination in a sample of electrons from bottom mesons, with the uncertainty coming from the strength of the gluonic corrections.

Let us next discuss the problems associated with determining the experimental jet axis. We suppose, for the sake of discussion, that the true jet axis J is displaced from the experimentally determined jet axis E by an angle δ, as shown in Fig. 9. Let $k_\perp$ and $k_{||}$ be the "true" transverse and longitudinal momenta of the electron with respect to the jet axis J. If we let $(k_\perp)_{\rm exp}$ be the transverse momentum with respect to the experimental jet axis E and ϕ_E be the angle between the plane determined by the electron momentum and the true jet axis, and the plane determined by the true and experimental axis, then

$$\langle k_\perp \rangle_{\rm exp} \equiv \frac{1}{2\pi}\int_0^{2\pi} d\phi_E (k_\perp)_{\rm exp} . \tag{3.9}$$

For $k_\perp$ large and δ small, we have

$$\langle k_\perp \rangle_{\rm exp} - k_\perp \cong \frac{\sin^2\delta}{4}\frac{2\cos^2\theta_J - \sin^2\theta_J}{\sin\theta_J} E_c . \tag{3.10}$$

In the above, θ_J is the angle that the electron's momentum makes with the true jet axis. For $k_\perp/k_{||}\sin\delta$ small, we have

$$\langle k_\perp \rangle_{\rm exp} - k_\perp \cong k_{||}\sin\delta + \frac{1}{4}\frac{k_\perp{}^2}{k_{||}\sin\delta} - k_\perp . \tag{3.11}$$

The region of applicability of (3.10) and (3.11) can be understood by examining Fig. 9. Consider first the case $\theta_J > \delta$. As ϕ_E varies between 0 and 2π, the angle between the experimental jet axis and the electron momentum is approximately θ_J; this is

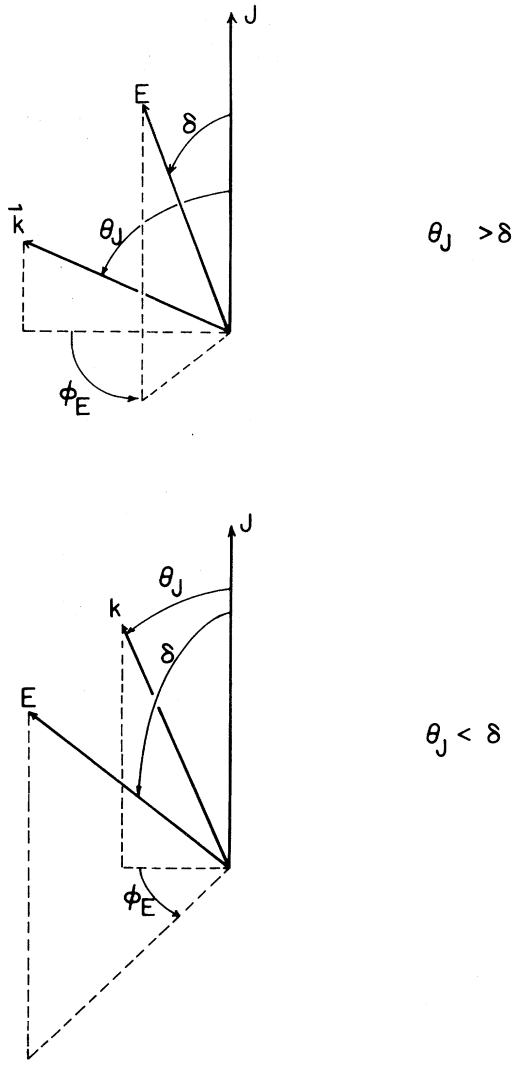

FIG. 9. Orientations of the true jet axis J, the experimental jet axis E, and the electron momentum $\vec{k}$.

suggested by Eq. (3.10). On the other hand, if $\theta_J < \delta$, then as we vary ϕ_E, the angle between the electron momentum and the experimental jet axis is approximately δ, as given by Eq. (3.11). The meaning of (3.10) and (3.11) is clear; electrons emitted at large angles with respect to the jet axis have a transverse-momentum spectrum that is relatively independent of experimental uncertainties in the location of the jet axis. On the other hand, electrons making small angles with respect to the jet axis have a transverse-momentum distribution that is dominated by experimental errors, rather than dynamics.

Fortunately, our high-transverse-momentum methods are insensitive to these experimental difficulties. To show this let us obtain an upper bound to the smearing in $k_\perp$. Consider an electron with $k_\perp = 1.2$ GeV/c. From Fig. 1 we see that at $\sqrt{s} = 31$ GeV 80% of all electrons have $E_c < 4.0$ GeV. So, we consider a case of large smearing by considering an event with an electron of energy 4.0 GeV. Let us assume that there is a very large error in locating the jet axis, setting $\delta = 10°$. If we insert these parameters into Eq. (3.10), we get

$$\langle k_\perp \rangle_{\text{exp}} - k_\perp = 0.19 \text{ GeV}/c \ . \tag{3.12}$$

Clearly, the above is a rough estimate of the actual smearing. If we assume a realistic distribution in δ, the shift in (3.12) will be much lower. Also, systematic effects such as high-$k_\perp$ electrons tending to have small $k_{||}$ will reduce (3.12) even further.

Having shown that major alterations in our scheme do not occur when one takes into account jet-axis uncertainty effects, we now make a quantitative estimate of the systematic effects due to the nonobservation of $\bar{\nu}$'s and K_L's in B and $\bar{D}$ decays. Our approach will be to compute the missing momentum due to the $\bar{\nu}$ or the $\bar{\nu}$ and K_L, and then estimate the orientation of the experimentally measured jet axis.

We consider the $\bar{D}$ semileptonic decay

$$\bar{D} \to e^- \bar{\nu} K \ ,$$

where K may be either pseudoscalar or vector, charged or neutral. If we use the pseudoscalar-vector ratio of 1:1, we can make an SU(3) estimate of the branching ratios, obtaining that the mode

$$\bar{D} \to e^- \bar{\nu} K_L + \text{hadrons} \tag{3.13}$$

occurs in $\frac{3}{8}$ of all $\bar{D}$ semileptonic decays. In the remainder of the decays, we assume

$$\bar{D} \to e^- \bar{\nu} + \text{observed hadrons} \ . \tag{3.14}$$

For simplicity, in (3.13) we assume that *only* the electron is observed, but in reaction (3.14), only the $\bar{\nu}$ is not observed. In this approximation, on an event-by-event basis, we can compute the missing three-momentum in the laboratory frame due to either the $\bar{\nu}$ or $\bar{\nu}K_L$ system, which we call $\vec{P}_x$.

In order to take into account the nonobservation of the missing neutrals, we take the experimental

thrust axis to be given by[5]

$$\vec{T}_E = \vec{T} - \vec{P}_x \ , \tag{3.15}$$

where

$$|T| = \frac{4+x}{3}\left[\frac{s}{4} - m_i^2\right]^{1/2} \ , \tag{3.16}$$

$\vec{T}$ is parallel to the direction of the heavy quark i, and m_i is the heavy quark mass.

Since in the actual analysis of hadronic events, one should add a "dummy" momentum vector to the set of observed hadron momentum vectors to guarantee momentum conservation,[21] the procedure that we describe does not reflect the actual deviation of the experimental jet axis from the "true" one that would arise in the analysis of an actual event. For example, if $|\vec{P}_x|$ is very large in comparison to the rest of the missing momentum, the dummy vector introduced into the analysis is approximately $\vec{P}_x$. In fact, if the K_L and $\bar{\nu}$ in (3.13) were the only missing neutral in the event, the dummy vector would be $\vec{P}_x$ exactly, and the experimental jet axis would be unaffected. A necessary condition for the missing neutrals to shift the direction of the thrust axis in a particular hadronic event is that there be soft hadrons distributed near the boundary of the hemispheres H_1 and H_2 which can "cross over" from one hemisphere to the other. (Of course, other types of situations such as those in which all the hadrons are generated with enormous $q_\perp$, are possible; our current understanding of jets suggest that such events are quite rare.) It should be clear the the thrust-axis uncertainty is dominated by the distribution of the soft hadrons, rather than the fast K_L's or $\bar{\nu}$'s. We feel that taking (3.15) as the experimental thrust axis overestimates the effects of the missing neutrals. We point out that sphericity, being quadratic in the particle momenta, does not share this property with thrust,[21] and is therefore not well suited for our type of analysis.

Our calculation of the jet-axis uncertainty effects for the B decays proceeds in an entirely analogous fashion. We take the $\bar{\nu}$ momentum as $\vec{P}_x$ throughout, due to the fact that the B mesons decay into states with high hadron multiplicity; the probability of a very large hadronic missing momentum is less likely than in the case of $\bar{D}$ decays.

In Figure 10, we show the effects of both hard-gluon bremsstrahlung and jet-axis uncertainty on the bottom electrons, as reflected in the distribution F_b in (3.5). In the preceding discussions, the electron $k_\perp$ distributions have been independent of our choice of $D(z)$ in (2.2), due to trivial kinematics. The smearing of the $k_\perp$ distribution due to the jet-axis uncertainty will now depend on the hardness of $D(z)$, as can be seen by examining (3.10). We expect that the BS distribution in (3.2) should experience a great deal of smearing, while the FF distribution in (3.2), considerably less. In Fig. 10, we see little difference in $F_b(k_\perp)$ for the BS (solid line) and FF (dashed line) fragmentation functions. The bottom electron distribution tends to be insensitive to experimental effects due to the fact that the B electrons tend to make relatively large angles with respect to the jet axis. In addition, the longitudinal-transverse-momentum correlations induced by gluon bremsstrahlung tend to produce high-$k_\perp$ electrons with low $k_{||}$. These correlations make the smearing due to experimental effects much less than would occur if the longitudinal-

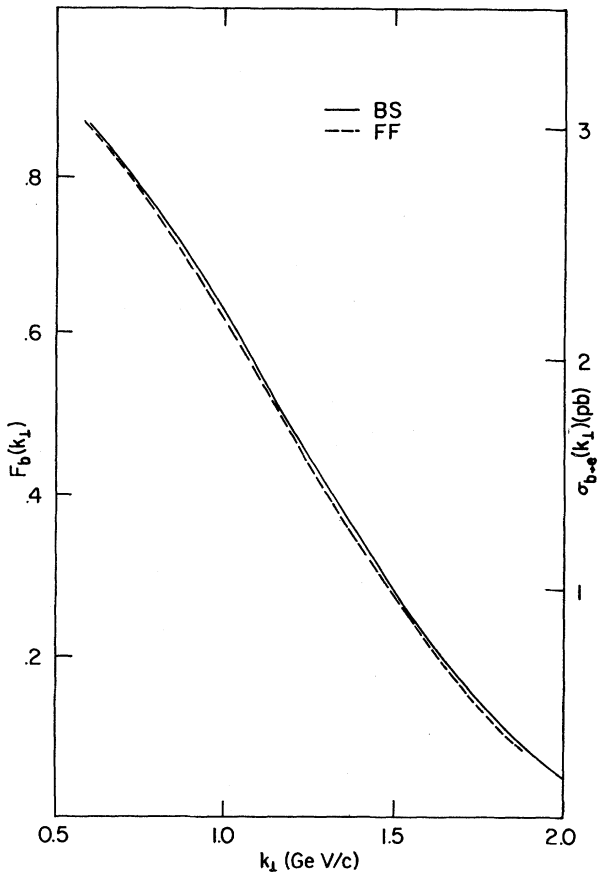

FIG. 10. Same as Fig. 3, but including gluon effects and jet-axis smearing. Solid line, BS. Dashed line, FF.

and transverse-momentum distributions generated by gluon emission actually factorized. In Fig. 8, curves X and Y show the cumulative effects of hard-gluon emission and experimental jet-axis smearing on the charm contamination function $I(k_\perp)$ defined in (3.6). Curve Y corresponds to the FF form for $D(z)$ [Eq. (3.1)] and curve Z corresponds to the choice $D(z)=1$. Since the experimental jet-axis smearing affects the electron charm distribution most strongly, the function $I(k_\perp)$ depends almost exclusively on the choice of fragmentation function for the $\bar{D}$. For a cut $k_\perp=1.2$ GeV/c, we get charm contaminations of less than 25% for constant, and less than 20% for FF fragmentation functions. If we assume a very soft longitudinal-momentum distribution, such as $D(z)=3(1-z)^2$, then the charm-contamination curve lies below curve Y.

To appreciate the importance of longitudinal-transverse momentum correlations, we point out that for $D(z)=1$, the value of $I(k_\perp)$ for 1.2 GeV/c grows from 24.4% to 28.8%, the increase coming from experimental jet-axis smearing effects. We believe that although the smearing of the $k_\perp$ distribution due to uncertainty in the location of the jet axis cannot be ignored, it certainly will not spoil our results.

IV. APPLICATIONS

In Sec. III we showed that experimental uncertainties, model dependences, etc., have little effect on our ability to isolate a clean signal of electrons at high $k_\perp$ arising from B-meson decay. Let us briefly mention some of the applications of these techniques.

A. Measurement of the b-quark production cross section.

Let us first address the problem of the level of measurability of the high-$k_\perp$ cross section. In Fig. 11, we show the prompt-electron cross section for $k_\perp > 1.2$ GeV/c, assuming the Gaussian parametrization of (2.5), with $t_H=0.45$ GeV/c. Over the PEP/PETRA energy range, we see that the prompt-electron cross section never drops below 1 pb (if one measures prompt positrons as well, we of course have a minimum of 2 pb). For different choices of the cut in $k_\perp$, the curve can be rescaled using Fig. 3. Note that the cross section is proportional to the electron branching ratio B_b.

Our discussion thus far has led us to the conclusion that the high-$k_\perp$ electrons provide a clean signal of B production, that may be accurately extrapolated to obtain the total B-production cross section using the formula[3]

$$\sigma_b=\frac{\sigma_{b\to e}(k_\perp)\,|_{\rm exp}}{B_b F_B(k_\perp)} \tag{4.1}$$

where $F_b(k_\perp)$ is the s-independent function given in (3.5), and $\sigma_{b\to e}(k_\perp)\,|_{\rm exp}$ is the observed high-$k_\perp$ cross section. The above formula would not be useful if the high-$k_\perp$ cross section were contaminated by large backgrounds.

B. Longitudinal-momentum distributions

We feel that a particularly novel application of our methods can be found in the study of the longitudinal-momentum distribution of the B's. In Fig. 12, we show curves for $d\sigma_e/dx_{||}$, where we have defined the electron fractional longitudinal momentum

$$x_{||}=\frac{2\,|k^c_{||}\,|}{\sqrt{s}}\ , \tag{4.2}$$

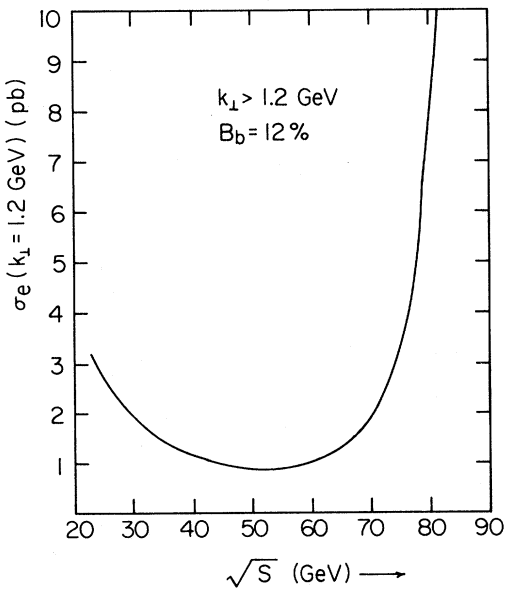

FIG. 11. Cross section for producing prompt electrons with $k_\perp > 1.2$ Gev/c.

where $k_{||}^c$ is the component of the electron's momentum parallel to the jet axis (notice that for the moment we do not distinguish between the quark direction and the antiquark direction). In Fig. 12(a) we display the $x_{||}$ distribution assuming FF (3.1) and BS (3.2) fragmentation functions for the B and $\bar{D}$'s. We obtain a slight difference for the two types of fragmentation functions, characterizing their different degrees of hardness, but the effects of bottom and charm are obviously difficult to separate. Furthermore, the two curves can only be distinguished with enormous statistics. We gain much better insight into the B fragmentation function by examining the $x_{||}$ distribution of high-$k_\perp$ electrons, shown in Fig. 12(b). The physical explanation is straightforward. In the rest frame of the B meson, the high-$k_\perp$ electrons are moving nearly perpendicular to the jet axis. If we Lorentz boost into the e^+e^- center-of-mass frame, the longitudinal momentum of the high-$k_\perp$ electrons is mainly generated by the Lorentz boost itself. The magnitude of the boost is directly proportional to the longitudinal momentum of the B. Therefore, the longitudinal momentum of the high-$k_\perp$ electron and the longitudinal momentum of the parent B are essentially proportional. As a result, we see the clear qualitative differences in the $x_{||}$ distributions shown in Fig. 12(b). The FF (3.1) fragmentation function describes a longitudinal-momentum distribution that is a decreasing function of z; as a result we see a sharp drop in the $x_{||}$ distribution as $x_{||}$ increases away from 0. On the other hand, the BS fragmentation function increases with z; thus we expect very few high-$k_\perp$ electrons with $x_{||}=0$, and the number should increase as $x_{||}$ gets large. The BS fragmentation function generates a distinctive "dip" at $x_{||}=0$. For comparison, we see that choosing $D(z)=1$ provides a relatively flat distribution at $x_{||}=0$, lying between FF and BS. From Eq. (3.10), we see that the spectrum near $x_{||}=0$ receives very little charm contamination due to uncertainties in determining the jet axis. We have calculated the $x_{||}$ spectrum, taking the thrust axis to be $\vec{T}_E$, as in (3.15). We find that although there is a rise in $d\sigma_e/dx_{||}$ for $x_{||}>0.2$, the low-$x_{||}$ spectrum is unaffected by experimental jet-axis-misidentification problems.

This picture is complicated somewhat when one considers the effects of hard-gluon bremsstrahlung. This may be understood by considering the case of $e^+e^-\to b\bar{b}G$. If the $\bar{b}$ and the gluon are both energetic, then the b quark is necessarily very soft. In such a situation, only a soft B meson can be produced, regardless of the form of the b-quark fragmentation function. Since soft-B mesons can give rise to high-$k_\perp$, low-$x_{||}$ electrons, hard-gluon emission is a mechanism for filling in the dip in Fig. 12(b). In Fig. 12(c), we show the effects of gluon bremsstrahlung and jet-axis smearing. The dashed curve, identical to that in Fig. 12(b), assumes the BS fragmentation function $t_H=0.45$ GeV/c, no gluon emission, and no jet-axis smearing. The solid curve corresponds to the BS hadronization, in addition to the inclusion of gluon events and jet-axis smearing. The crossed curve corresponds to the FF case, with gluons and jet-axis smearing taken into account. As expected, the gluon effects eliminate the dip at $x_{||}=0$. On the other hand, if we compare the FF case in Figs. 12(b) and 12(c), we see that the $x_{||}$ distribution is modified significantly only for $x_{||}<0.05$. We point out that the BS and FF fragmentation functions are still distinguishable. Since the rise in the small-x region for the BS case is exclusively due to gluon emission, the dip will be revealed, say, by a cut to exclude the three-jet events, if the b quark hadronizes according to a hard fragmentation function such as the BS. The high-$k_\perp$, low-$x_{||}$ cross section appears to be sensitive to the manner in which the cross section in (3.7) is regularized, and the study of this region may give some insight into the infrared behavior of QCD. Finally, we suggest that a high-$k_\perp$, low-$x_{||}$ electron trigger may be a useful way to isolate energetic gluon jets. We shall examine these points in a future work.

C. b-quark$-Z^0$-boson couplings

Another interesting application of our formalism is the study of the coupling of the b quark to the Z^0. In this subsection, we shall ignore gluon effects. From Fig. 11, we see that the Z^0 has little effect on the total cross section in the PETRA/PEP energy range. On the other hand, we expect a significant effect when we examine the angular asymmetry of the quark jet axis. In Ref. 8, a formalism was presented whereby the angular distribution of the thrust axis was calculated, where the quark jet was defined through the use of some specific "criterion." The quantities ω_i and $\bar{\omega}_i$ are the probabilities that the quark and antiquark jets, respectively, satisfy our criteria. If we let our criterion for choosing the quark jet direction be that the prompt electron has a positive component of $\vec{k}$ along the thrust axis in the quark direction, we have, for the b quark,

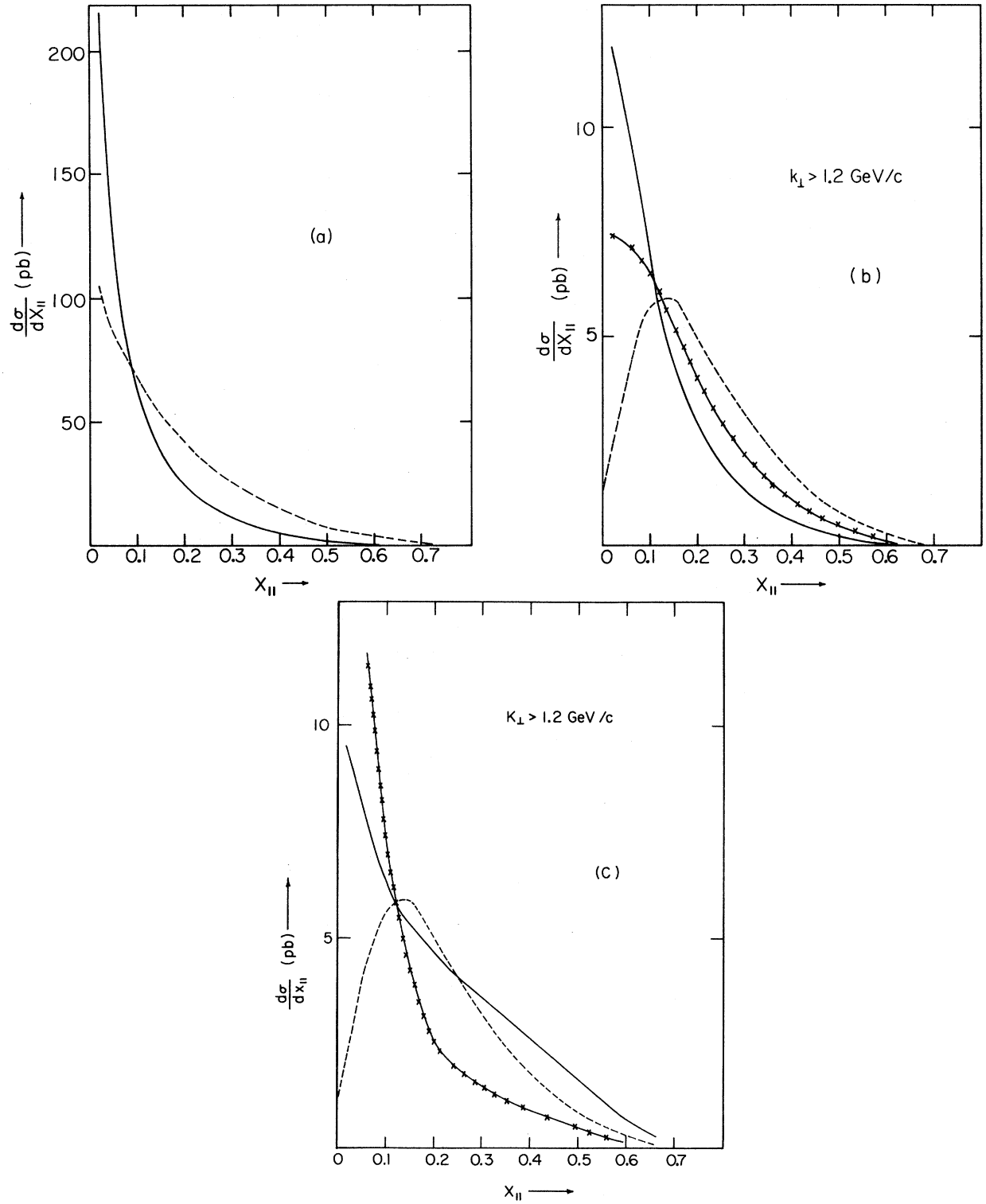

FIG. 12. (a) Fractional longitudinal-momentum spectrum of prompt electrons. Solid line: FF fragmentation function. Dashed line: BS fragmentation (primordial smearing only). (b) Same for prompt electrons with $k_\perp > 1.2$ GeV/c. Solid line: FF. Dashed line: BS. Cross line: constant fragmentation function $D(z)=1$ (primordial smearing only). (c) Same for prompt electrons with $k_\perp > 1.2$ GeV/c. Dashed line: BS. Solid line: BS, with gluons and jet-axis smearing. Crossed line: FF, with gluons and jet-axis smearing.

$$\omega_b = \int_0^1 d(\cos\theta_J)\frac{1}{\sigma_b}\left[\frac{d\sigma_{b\to e}}{d(\cos\theta_J)}+\frac{d\sigma_{\bar{b}\to\bar{c}\to e}}{d(\cos\theta_J)}\right], \tag{4.3}$$

$$\bar{\omega}_b = \int_{-1}^0 d(\cos\theta_J)\frac{1}{\sigma_b}\left[\frac{d\sigma_{b\to e}}{(\cos\theta_J)}+\frac{d\sigma_{\bar{b}\to\bar{c}\to e}}{d(\cos\theta_J)}\right],$$

and for the charm quark,

$$\omega_c = \int_0^1 d(\cos\theta_J)\frac{1}{\sigma_c}\frac{d\sigma_{\bar{c}\to e}}{d(\cos\theta_J)}, \tag{4.4}$$

$$\bar{\omega}_c = \int_{-1}^0 d(\cos\theta_J)\frac{1}{\sigma_c}\frac{d\sigma_{\bar{c}\to e}}{d(\cos\theta_J)}.$$

In the above, θ_J is the angle between the prompt-electron momentum and the quark jet axis; $\theta_J=\pi$ corresponds to the case of the electron moving parallel to the antiquark. The above quantities clearly must depend on the function $D_i(z)$. For example, if the b longitudinal-momentum distribution is peaked near $z=1$, it is less likely that an electron will have $k_{||}$ pointing in the $\bar{b}$ direction than it would be for $D_i(z)$ peaked near $z=0$. If we restrict ourselves to the case of electrons with $k_\perp > 1.2$ GeV/c, we have the following results for $\sqrt{s}=31$ GeV:

Field-Feynman: $\omega_b=0.049$, (4.5)

$\bar{\omega}_b=0.010$;

Bjorken-Suzuki: $\omega_b=0.054$, (4.6)

$\bar{\omega}=0.005$;

Soft, $D(z)=3(1-z)^2$: $\omega_b=0.046$, (4.7)

$\bar{\omega}_b=0.013$.

In all cases, ω_c, $\bar{\omega}_c$ are negligible. The experimentally observed asymmetry $\tilde{A}$ is given in terms of the theoretical b-quark asymmetry $\tilde{A}_b$ through the relation[8]

$$\tilde{A}=\frac{\omega_b-\bar{\omega}_b}{\omega_b+\bar{\omega}_b}\tilde{A}_b. \tag{4.8}$$

The above is slightly different from the formula in Ref. 8, due to the fact that it is impossible to simultaneously emit an electron in the quark and the antiquark direction. Since $\tilde{A}_b=-0.178$ at $\sqrt{s}=31$ GeV,[8] we have

Field-Feynman: $\tilde{A}=-0.12$, (4.9)

Bjorken-Suzuki: $\tilde{A}=-0.15$,

soft, $D(z)=3(1-z)^2$: $\tilde{A}=-0.10$.

It should be obvious that in addition to giving us information about the couplings of the Z^0 to quarks, the prompt-lepton asymmetries will provide additional constraints on the quark fragmentation models. We explore these and other effects in detail in a separate work.[22]

V. CONCLUSIONS

Let us summarize the main results of our work. We have shown that prompt electrons from B-meson decays produce a distinctive signal at high $k_\perp$ with respect to the jet axis. The corresponding cross section is easily measurable, and with small background from other sources. The shape of the high-$k_\perp$ electron spectrum is insensitive to assumptions regarding vector-meson production, primordial transverse momentum of the hadrons, and experimental uncertainties in locating the jet axis. We can extrapolate the high-$k_\perp$ spectrum to obtain the b-quark production cross section. We can study the longitudinal-momentum distribution of the B meson, and distinguish hard longitudinal-momentum distributions of the type suggested by Bjorken and Suzuki from softer distributions, without reconstructing the B from its decay products. Finally, we can study the coupling of the b quark to the Z^0 boson by investigating the angular asymmetry in the thrust-axis distribution.

ACKNOWLEDGMENTS

We would like to thank our colleagues at Ames Laboratory for continuing interest in the present work, and in particular Jerry Lamsa, for a useful discussion. We also wish to thank Gary Feldman for helpful suggestions. This work was supported, in part, by the U. S. Department of Energy, Contract No. W-7405-eng-82, Office of Basic Science (KA-01-01), Division of High Energy Physics and Nuclear Physics.

*On leave of absence from Warsaw University Branch at Bialystok, Poland.
†Visiting scientist at Iowa State University from Zhejiang University, Hangzhou, Zhejiang, The People's Republic of China.

[1]D. Andrews *et al.*, Phys. Rev. Lett. 45, 219 (1980); G. Finocchiaro *et al., ibid.* 45, 222 (1980).
[2]C. Bebek *et al.*, Phys. Rev. Lett. 46, 84 (1981); K. Chadwick *et al., ibid.* 46, 88 (1981).
[3]M. J. Puhala, Z. J. Rek, B.-L. Young, and X. T. Zhu, Phys. Lett. B (to be published).
[4]V. Barger *et al.*, Phys. Rev. D 16, 746 (1978).
[5]For a detailed account of the calculation, see M. J. Puhala, Z. J. Rek, B.-L. Young, and X. T. Zhu, Ames Laboratory Report No. IS-J 534 (unpublished).
[6]M. Gronau *et al.*, Nucl. Phys. B123, 47 (1977).
[7]A. Ali, Z. Phys. C 1, 25 (1979).
[8]M. J. Puhala, Z. J. Rek, and B. L. Young, Phys. Rev. D 23, 89 (1981).
[9]J. Ellis, M. K. Gaillard, and G. G. Ross, Nucl. Phys. B111, 253 (1976); B130, 516(E) (1977).
[10]A. Ali and E. Pietarinen, Nucl. Phys. B154, 519 (1979).
[11]M. Kobayashi and K. Maskawa, Prog. Theor. Phys. 49, 652 (1973).
[12]R. E. Shrock, S. B. Treiman, and L. L. Wang, Phys. Rev. Lett. 42, 1589 (1979); V. L. Barger, W. F. Long, and S. Pakvasa, *ibid.* 42, 1585 (1979). We have used the parameters given in the former.
[13]J. Kirkby, in *Proceedings of the 1979 International Symposium on Lepton and Photon Interactions at High Energies, Fermilab,* edited by T. B. W. Kirk and H. D. I. Abarbanel (Fermilab, Batavia, Illinois, 1980), p. 107.
[14]R. D. Field and R. P. Feynman, Nucl. Phys. B136, 1 (1978).
[15]Talks by S. L. Wu and S. Yamada, in *High Energy Physics—1980,* proceedings of the XX International Conference, Madison, Wisconsin, edited by L. Durand and L. Pondrom (AIP, New York, 1981), pp. 604, 616.
[16]J. D. Bjorken, Phys. Rev. D 17, 171 (1978); M. Suzuki, Phys. Lett. 71B, 139 (1977).
[17]G. Wolf, Report No. DESY 80/13 (unpublished).
[18]B. L. Ioffe, Phys. Lett. 78B, 227 (1978).
[19]P. Hoyer *et al.*, Nucl. Phys. B161, 349 (1979); A. Ali. *et al.*, Phys. Lett. 93B, 155 (1980).
[20]G. Wolf, in proceedings of the Summer Institute on Particle Physics, SLAC, 1980, edited by Anne Mosher (SLAC, Stanford, 1981).
[21]S. Brandt and H. D. Dahmen, Z. Phys. C 1, 61 (1979).
[22]M. J. Puhala, Z. J. Rek, B.-L. Young, and X.-T. Zhu, Phys. Rev D 25, 95 (1982).
[23]R. Brandelik *et al.*, Phys. Lett. 89B, 418 (1980).